Mapping of Retinal Projections in the Living Rat Using High-Resolution 3D Gradient-Echo MRI With Mn^{2+}-Induced Contrast

Takashi Watanabe, Thomas Michaelis,* and Jens Frahm

This study describes the neuroaxonal tracing of the visual pathway in the living rat using high-resolution T_1-weighted 3D gradient-echo MRI (195 × 195 × 125 μm^3) at 8, 24, 48, and 72 h after intraocular Mn^{2+} injection (0.1 μl of 1 M aqueous $MnCl_2$). Best results were obtained at 24 h postinjection, revealing a continuous pattern of anterograde labeling from the retina, optic nerve, and chiasm to the contralateral optic tract, the dorsal and ventral lateral geniculate nucleus, the superior colliculus and its brachium, the olivary pretectal nucleus, the nucleus of the optic tract, and the suprachiasmatic nucleus. These results underline the feasibility of repeated MRI tract tracing in living animals after a single injection of Mn^{2+}. The approach is expected to advance studies of neuroaxonal function in behaving animals with special emphasis on applications in developmental neurobiology. Magn Reson Med 46:424–429, 2001.

Key words: magnetic resonance imaging; retinal projection; manganese; neuroanatomic tract tracing

In the visual system of mammals, which have eyes placed far laterally on the head, the great majority of the optic nerve fibers decussate at the chiasm (1). The fibers then enter the optic tract, which projects to three main subcortical targets (2,3): the lateral geniculate nucleus processes visual information that ultimately results in visual perception; the pretectal area of the midbrain uses retinal input to produce pupillary reflexes; and the superior colliculus generates eye movements (4). In addition, there is a direct retinohypothalamic projection to the suprachiasmatic nucleus (5,6) as the principal circadian pacemaker in mammals, which is responsible for the generation and regulation of rhythms in behavioral state, performance, hormonal secretion, and physiologic function (7–9).

Conventional neuroanatomic techniques for tract tracing rely on sectioning of the brain and therefore preclude repeated measurements of the same animal. However, a method which is based on neuronal uptake and axonal transport of a suitable tracer compound can provide access to the neuroaxonal connectivity and, therefore, may develop into a functional tool that allows for multiple examinations of a specific tract in a living animal, e.g., at different stages after labeling or in response to various sensory or cognitive inputs. Considering this perspective, Pautler et al. (10) introduced manganese-enhanced MRI as an alternative method for neural tracing. The method utilizes free unchelated manganese ions (Mn^{2+}) which, analogous to calcium ions (Ca^{2+}), are taken up by neurons and transported along axons.

Mn^{2+} has long been used as an MRI contrast agent because the paramagnetic ion affects the longitudinal relaxation rate ($1/T_1$) of surrounding water protons (11). Provided that Mn^{2+} remains compartmentalized after exogenous administration, it can be used for delineating targeted tissue elements. In fact, Sloot and Gramsbergen (12) provided evidence for the neuronal uptake and anterograde axonal transport of radioactive Mn^{2+} after microinjection into the rat basal ganglia by revealing a region-specific accumulation and retention for at least 72 h. Pautler et al. (10) demonstrated T_1-weighted signal enhancement of the olfactory pathway after topical administration of $MnCl_2$ to the naris of mice as well as of the contralateral optic tract after intravitreal injection into a single eye. Extending neuroaxonal tract tracing in murine brain in situ, the purpose of the present work was to develop an in vivo protocol suitable for repeated studies of the visual pathway of behaving rodents using high-resolution 3D gradient-echo MRI with manganese-induced contrast.

MATERIALS AND METHODS

Animals and Mn^{2+} Administration

A total of seven 16-week-old female albino Wistar rats (250–290 g) were studied in accordance with German animal protection laws after approval by the responsible governmental authority. Animals were fasted for 12 h before each anesthetic procedure but were allowed free access to water. Anesthesia was induced by 2.0–4.0% halothane in a 7:3 mixture of N_2O and O_2. After being relaxed, the animals were intubated under visual control (laryngoscope, Aesculap AN404, Eickemeyer, Germany) with a purpose-built endotracheal tube (1.4 mm i.d., 2.1 mm o.d.), and artificially ventilated with an animal respirator (Rhema, Germany). Anesthesia was maintained using 1.5% halothane in a 7:3 mixture of N_2O and O_2.

Intraocular injection of Mn^{2+} was performed with a purpose-built 27-gauge needle (17 mm length) connected via a polyethylene tube (70 mm length, 0.4 mm i.d., Portex, UK) to a 5 μl Hamilton syringe (#710-N). The anesthetized animals were placed in a prone position. The tip of the needle was inserted into the vitreous body of the left eye with the aid of a microscope. The insertion site was about 2 mm posterior to the dorsal limbus. Proper placement of the needle was verified by observing the magnified image of the tip through the lens of the animal's eye. A 0.1 μl volume of a 1 M aqueous solution of $MnCl_2$ (Sigma, Taufkirchen, Germany) was injected into the vitreous body

Biomedizinische NMR Forschungs GmbH am Max-Planck-Institut für biophysikalische Chemie, Göttingen, Germany.

*Correspondence to: T. Michaelis, Ph.D., Biomedizinische NMR Forschungs GmbH, 37070 Göttingen, Germany. E-mail: tmichae@gwdg.de

Received 31 January 2001; revised 19 May 2001; accepted 23 May 2001.

of the left eye over a 5-min period. The amount was estimated by calibrating the advancement of the meniscus in the polyethylene tube with the scale of the Hamilton syringe. The needle was left in place for 15 min and then slowly withdrawn to minimize the loss of $MnCl_2$ from leakage at the injection site. This waiting period was found to be necessary with regard to a distribution of the $MnCl_2$ solution and the equilibration of the intraocular pressure. Anesthesia was terminated and the animals were returned to their cages.

One of the animals presented with a clouded vitreous body—most likely due to mechanical damage and bleeding—and was euthanized. The remaining six animals did not appear to be in any distress. When light was shone upon the injected eye, it caused constriction of the pupil. Four animals participated in the Mn^{2+} time-course study; two animals were examined at 24 h after injection.

MRI

MRI studies were performed at 8, 24, 48, and 72 h after Mn^{2+} administration. The animals were anesthetized as described above and placed in the magnet bore in a supine position with the heads firmly fixed. A heated water blanket and bed were used to maintain rectal body temperature at 37 ± 1°C. To monitor both breathing frequency and amplitude, the respiration signal of a water-filled balloon attached to the animal's chest was detected using a pressure transducer (P23 ID, Statham Medical Instruments, Hato Ray, Puerto Rico). After each measurement the animals were revived from anesthesia, placed in their cages with free access to food and water, and held under a 12/12 h light/dark regimen.

All measurements were carried out at 2.35T using an MRBR 4.7/400 mm magnet (Magnex Scientific, Abingdon, UK) and a DBX system (Bruker Medical GmbH, Ettlingen, Germany) equipped with B-GA20 gradients (200 mm i.d., 100 mT m^{-1} maximum gradient strength). RF excitation and signal reception were accomplished with the use of a birdcage coil (154 mm i.d.) and a saddle-shaped surface coil (40 mm diameter), respectively (Bruker Medical).

Proper positioning of the head was ensured by coronal and sagittal multislice gradient-echo images (RF-spoiled FLASH, TR/TE = 150/5 ms, flip angle 20°). High-resolution MRI datasets were acquired using a T_1-weighted 3D gradient-echo sequence (RF-spoiled 3D FLASH, TR/TE = 15/4.2 ms) with a flip angle of 25°, which was found to yield better contrast-to-noise than 15° or 35° excitations for otherwise identical conditions (pilot studies at 24 h after injection). The use of a 50-mm FOV along both the rostrocaudal and left-to-right direction and a 16-mm FOV along the dorsal–ventral direction in conjunction with an acquisition matrix of 256 × 256 × 128 complex data points resulted in a voxel resolution of 195 × 195 × 125 μm^3. Neither zero-filling nor filtering were applied. The measuring time was 65.5 min (eight averages).

Image Analysis

Bruker's Paravision software for multiplanar reconstructions from 3D MRI datasets was applied to extract identical anatomic sections from examinations of the same animal at different times after Mn^{2+} injection. The 'stereotactic' procedure involved the definition of three orthogonal reference sections with respect to neuroanatomic landmarks of the skull and the brain. As shown in Fig. 1, a sagittal reference plane bisected the two hemispheres of the brain while following the superior longitudinal sinus. Subsequently, a perpendicular transverse reference plane was defined which touched the frontal and parietal vertex of the skull. Finally, a coronal reference plane, perpendicular to both other planes, was defined to cut through the posterior commissure with the habenular commissure just rostral to the section. Following this procedure, all 3D MRI datasets obtained in this study demonstrated the mammillary body just rostral and the central interpeduncular nucleus caudal to the coronal reference plane.

In addition, the software allowed the calculation of maximum intensity projections of enhanced structures onto arbitrarily oriented planes. Because projections in the left–right and dorso–ventral direction were superimposed by high intensities from fat and vessels, the full length of the enhanced visual pathway was best depicted in a rostrocaudal projection.

RESULTS

All animals revealed a pronounced anterograde Mn^{2+} enhancement that—together with the achieved spatial resolution—enabled a detailed examination of the rat retinal projections, including terminal fields. Apart from a weak unspecific signal increase in cortical and subcortical regions, the T_1-weighted 3D gradient-echo images at 24 h postinjection shown in Fig. 2 depict a clear delineation of

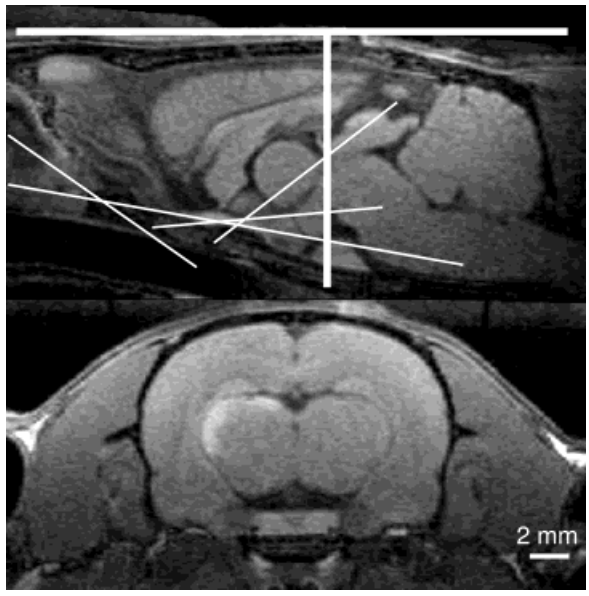

FIG. 1. Sagittal (top) and coronal section (bottom) of a rat brain (24 h after Mn^{2+}-injection into the left eye) defining the positions of four transverse-to-coronal sections selected for Fig. 2 relative to two orthogonal reference planes (thick lines), which have been introduced for an intraindividual follow-up of enhanced structures independent of the orientation of the 3D gradient-echo MRI dataset (spatial resolution 195 × 195 × 125 μm^3).

the retina, the axonal tracts, and the primary visual centers.

Figure 3 presents maximum intensity projections of the Mn^{2+}-enhanced 3D MRI data along the rostro-caudal direction obtained at various stages after injection. The best enhancement of the visual pathway, in terms of signal contrast and anatomic continuity, was achieved at 24 h postinjection. Early datasets (8 h postinjection) exhibited only insufficient transport of Mn^{2+} beyond the optic chiasm, while late examinations (48 h postinjection or later) suffered from fading contrast. It should be noted, however, that the axonal terminal areas showed less decline of the Mn^{2+}-induced contrast between 24 and 72 h postinjection than the optic tract, which represents the projecting portion of the axons. A quantitative analysis of structures with increasing distance from the injection site confirms these observations. Table 1 summarizes the SNR, defined as mean pixel intensity divided by the standard deviation of the noise, in standardized regions-of-interest (ROIs) of the rat brain as a function of time after Mn^{2+} administration. Values from individual cross-sectional images were obtained for enhanced elements of the visual pathway, including the left optic nerve (nearest to the injection site: 9.0 mm rostral to the coronal reference plane, 0.2 mm^2 ROI), the contralateral optic tract (medial distance: 3.0 mm rostral, 0.34 mm^2 ROI) and the contralateral superior colliculus (largest distance: 2.1 mm caudal, 0.57 mm^2 ROI) as well as for control regions in the cortex and basal ganglia (3.0 mm rostral, 0.95 mm^2 ROI each). Taking the difference of the SNR values for enhanced structures and control regions as a measure for the Mn^{2+}-induced contrast yields a maximum differential enhancement for the entire visual pathway at 24 h postinjection.

Figure 4 indicates the anatomic positions of four coronal sections, which are displayed in Fig. 5 for a more detailed delineation of the individual elements of the visual pathway. These sections were positioned using the coronal reference plane defined in Fig. 1. They demonstrate the course of labeled fibers through the right optic tract to the thalamus, highlighting both the dorsal and lateral portion of the ventral lateral geniculate nucleus. Their continuation passes the brachium of the superior colliculus to reach the midbrain, where they should have extensive terminal arborizations. The pretectal region showed strong enhancement in the form of a gently curved band. Rostrally, this band presents with an oval shape in coronal sections, which identifies the olivary pretectal nucleus with a particularly strong enhancement in the medial portion of the nucleus. At the level of the posterior pole of the lateral geniculate body, dense labeling was observed at an anatomic position where the brachium of the superior colliculus should enter the stratum opticum laterally. The underlying structure is assigned to the nucleus of the optic tract.

With respect to the superior colliculi, the Mn^{2+} enhancement mainly occurred on the side contralateral to the injected eye involving the whole superficial gray layer. The observation of some ipsilateral tectal anterograde la-

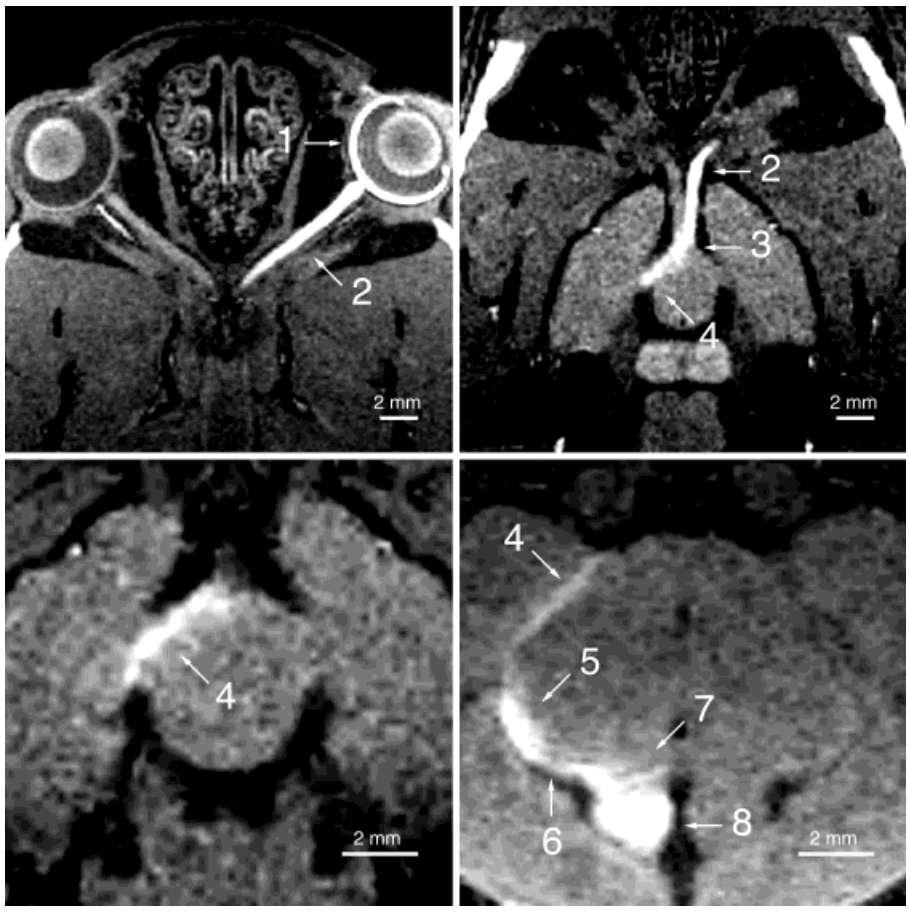

FIG. 2. Signal enhancement of the rat visual pathway (24 h after Mn^{2+}-injection into the left eye) in oblique sections −35° (top left), −10° (top right), +5° (bottom left), and +37.5° (bottom right) relative to the transverse reference plane shown in Fig. 1 (sections indicated in Fig. 1). Enhanced structures are: (1) left retina, (2) left optic nerve, (3) optic chiasm, (4) right optic tract, (5) right lateral geniculate nucleus, (6) right brachium of the superior colliculus, (7) right pretectal region, and (8) right superior colliculus.

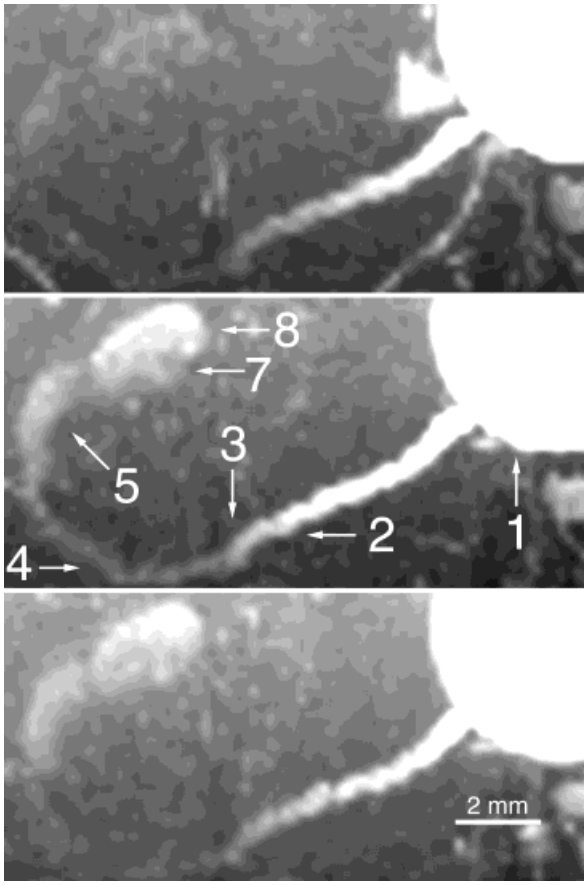

FIG. 3. Maximum intensity projections (rostro-to-caudal view) of the visual pathway in the same rat at 8 h (top), 24 h (middle), and 48 h (bottom) after Mn^{2+}-injection into the left eye. Anatomic labeling as in Fig. 2.

beling appears to affect only the superficial portion of this layer. Finally, the data provided substantial evidence for the retinohypothalamic tract yielding bilateral labeling of the suprachiasmatic nuclei. The enhancement was slightly more pronounced and longer-lasting in the contralateral hemisphere.

The sequential acquisition of 3D MRI datasets allowed a rough estimate of the velocity of Mn^{2+} enhancement along the projection fibers. For example, a weak but unequivocal

Table 1
SNRs of Manganese-Enhanced Structures Along the Rat Visual Pathway and Control Regions After Mn^{2+} Injection Into the Left Eye

Region	8 h*	24 h	48 h	72 h*
Left optic nerve	22.0 ± 0.7	25.0 ± 3.9	22.6 ± 3.1	20.1 ± 4.4
Right optic tract	18.2 ± 2.1	19.5 ± 2.0	18.9 ± 1.6	17.7 ± 1.8
Right superior colliculus	26.9 ± 1.5	32.0 ± 1.9	29.1 ± 3.3	28.8 ± 3.3
Cortex	19.1 ± 1.1	18.5 ± 1.7	19.2 ± 0.8	18.4 ± 1.9
Basal ganglia	17.1 ± 0.8	16.6 ± 1.1	17.4 ± 1.1	16.9 ± 0.5

The data represent mean values ± SD ($n = 4$) averaged across animals (*$n = 3$).

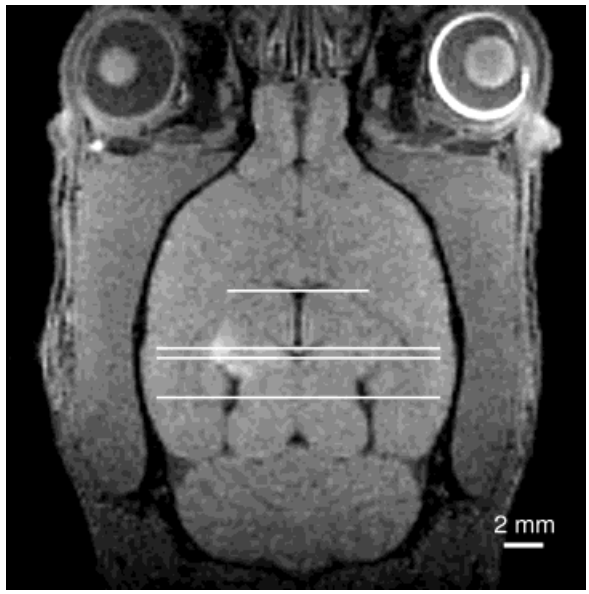

FIG. 4. Transverse section of a rat brain (24 h after Mn^{2+}-injection into the left eye, 5.8 mm below the transverse reference plane shown in Fig. 1) defining the positions and magnifications of four coronal sections selected for Fig. 5.

enhancement of the superior colliculus was detected about 8 h after Mn^{2+} administration in all animals (n = 3). From the 3D MRI data the length of the pathway from the optic disc to the superior colliculus was determined to be 22.5 ± 0.9 mm, yielding a speed of about 2.8 mm h^{-1}.

DISCUSSION

The present results confirm and extend recent work by Pautler et al. (10) on Mn^{2+} as an MRI-detectable tracer for neural tracts. In particular, the data demonstrate the usefulness of Mn^{2+} as an anterograde tracer, which labels neural connections over long distances and time periods in a manner readily detectable by repeated in vivo MRI at high spatial resolution. This possibility allows for the assessment of neuroaxonal functions in behaving animals, which among other applications promises new insights into the relevance of specific genetic modifications, e.g., when comparing normal with mutant or 'knockout' animals. In addition, the recent mapping of regional brain functions via an activation-induced accumulation of Mn^{2+} after breaking the blood–brain barrier during task performance further supports the notion that pertinent techniques indeed measure calcium-dependent synaptic activity (13,14).

The observed pattern of Mn^{2+} enhancement describes the primary optic centers at high spatial resolution and in excellent agreement with previous non-NMR studies of anterograde tracing (2,3,6,15). In this respect, the use of high-resolution 3D MRI datasets in conjunction with a postacquisition stereotactic reconstruction of identical anatomic planes for intraindividual comparisons proved to be of particular value. Nevertheless, it should be acknowledged that the achieved voxel volume of 4.75 nL still unfavorably compares with traditional light, fluorescence,

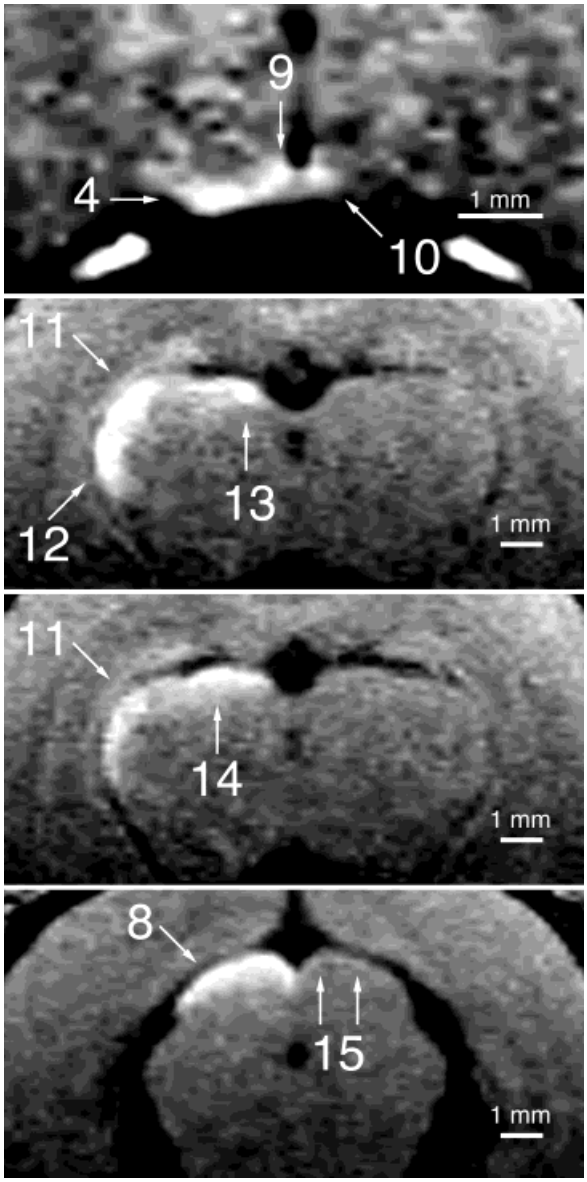

FIG. 5. Signal enhancement of individual components of the rat visual pathway (24 h after Mn^{2+}-injection into the left eye) in sections 4.3 mm rostral (top) as well as 0.2 mm rostral, 0.1 mm caudal, and 2.1 mm caudal (bottom) to the coronal reference plane shown in Fig. 1 (sections indicated in Fig. 4). Anatomical structures are labeled as in Fig. 2 with the following additions: (9) right and (10) left suprachiasmatic nucleus, (11) right dorsal and (12) ventral lateral geniculate nucleus, (13) right olivary pretectal nucleus, (14) right nucleus of the optic tract, and (15) superficial part of the superficial gray layer of the left superior colliculus.

or electron microscopy techniques. Although a reduction in MRI voxel volume by about one order of magnitude is technically feasible, such studies require significantly prolonged measuring times and possibly the preparation of fixed in vitro specimens.

A shortcoming of MRI-based neuroanatomic tracing is its relatively low sensitivity. Several tracts known to consist of only a few fiber connections can be visualized by other methods but were not distinguishable in this study, e.g., the nuclei of the accessory optic system as well as the lateral geniculate and olivary pretectal nuclei in the ipsilateral brain. Furthermore, the data did not reveal any evidence for transsynaptic crossing of Mn^{2+}, although previous studies of the rodent olfactory pathway suggested that Mn^{2+} can jump across a synapse (10,16). In the present study signal enhancement was confined to regions known to directly project from the retina; no enhancement was observed in visual cortical areas. It remains unclear whether this situation results from a dilution of the local Mn^{2+} concentration. Although multiple injections are possible, they may also cause a more pronounced unspecific enhancement, as Mn^{2+} may be released from the axon terminals in the primary optic centers or the systemic circulation after absorption by the capillary vessels in the retina. Previous work also indicated that Mn^{2+} uptake into the olfactory epithelium and transfer to the olfactory bulb along the primary olfactory neurons is a saturable process (16). If this applies to the uptake of Mn^{2+} by the retinal ganglion cell or the transport along its axon, the locally achievable concentration may be the limiting factor determining the MRI contrast for neural tracing.

Since the first quantitative study of axonal flow in rodent optic nerve fibers was presented (17), a large body of work has revealed the basic phenomena of transport in axons, including the observation of organelle transport in living neurons and pulse-labeling studies of protein synthesis (18). In this perspective, the key advantage of MRI is the in vivo applicability for mapping neuroaxonal connections in the intact brain. The method relies on the neurochemical similarity of Mn^{2+} to Ca^{2+}, which allows Mn^{2+} to enter neurons through Ca^{2+} channels during neuronal depolarization (19,20). Retinal ganglion cells of the rat have indeed been demonstrated to express several types of ligand-gated ion channels with a high permeability for Ca^{2+} (21).

The velocity of about 2.8 mm h^{-1} estimated for Mn^{2+} enhancement from the retina to the superior colliculus includes both the uptake of Mn^{2+} by the retinal ganglion cell and the subsequent transport along the axon. Nevertheless, the velocity is within the range of neuroaxonal transport rates of about 2 mm h^{-1} obtained for optic nerve fibers in mice (10) and 2.9 mm h^{-1} reported for primary olfactory neurons in pikes (22). Because mammalian nerves exhibit two major processes which move material from the cell body to the nerve terminal with very different rate constants, it may be concluded that at 24 h after injection the predominant contribution to the axonal transport of Mn^{2+} stems from the 'fast' component (2–16 mm h^{-1}) previously ascribed to the movement of membranous organelles along microtubules in rat retinal ganglion cell axons (23).

REFERENCES

1. Voogd J. Visual system. In: Nieuwenhuys R, Ten Donkelaar HJ, Nicholson C, editors. The central nervous system of vertebrates. Heidelberg: Springer-Verlag; 1998. p 1791–1820.
2. Hayhow WR, Sefton A, Webb C. Primary optic centers of the rat in relation to the terminal distribution of the crossed and uncrossed optic nerve fibers. J Comp Neurol 1962;118:295–321.
3. Toga AW, Collins RC. Metabolic response of optic centers to visual stimuli in the albino rat: anatomical and physiological considerations. J Comp Neurol 1981;199:443–464.

4. Mason C, Kandel ER. Central visual pathways. In: Kandel ER, Schwartz JH, Jessell TM, editors. Principles of neural science, 3rd ed. New York: Elsevier; 1991. p 420–439.
5. Moore RY, Lenn NJ. A retinohypothalamic projection in the rat. J Comp Neurol 1972;146:1–14.
6. Johnson RF, Morin LP, Moore RF. Retinohypothalamic projections in the hamster and rat demonstrated using cholera toxin. Brain Res 1988; 462:301–312.
7. Klein DC, Moore RY, Reppert SM. Suprachiasmatic nucleus: the mind's clock. New York: Oxford University Press; 1991.
8. Meijer JH, Rietveld WJ. Neurophysiology of the suprachiasmatic pacemaker in rodents. Physiol Rev 1989;69:671–707.
9. Miller JD, Morin LP, Schwartz W J, Moore RY. New insights into the mammalian circadian clock. Sleep 1996;19:641–667.
10. Pautler RG, Silva AC, Koretsky AP. In vivo neuronal tract tracing using manganese-enhanced magnetic resonance imaging. Magn Reson Med 1998;40:740–748.
11. Lauterbur PC, Mendonca-Dias MH, Rudin AM. Augmentation of tissue water proton spin-lattice relaxation rates by in vivo addition of paramagnetic ions. In: Dutton PL, Leigh LS, Scarpaa A, editors. Frontier of biological energetics. New York: Academic Press; 1978. p 752–759.
12. Sloot WN, Gramsbergen JP. Axonal transport of manganese and its relevance to selective neurotoxicity in the rat basal ganglia. Brain Res 1994;657:124–132.
13. Lin YJ, Koretsky AP. Manganese ion enhances T_1-weighted MRI during brain activation: an approach to direct imaging of brain function. Magn Reson Med 1997;38:378–388.
14. Duong TQ, Silva AC, Lee AP, Kim SG. Functional MRI of calcium-dependent synaptic activity: cross correlation with CBF and BOLD measurements. Magn Reson Med 2000;43:383–392.
15. Beckstead RM, Frankfurter A. A direct projection from the retina to the intermediate gray layer of the superior colliculus demonstrated by anterograde transport of horseradish peroxidase in monkey, cat and rat. Exp Brain Res 1983;52:261–268.
16. Henriksson J, Tallkvist J, Tjälve H. Transport of manganese via the olfactory pathway in rats: dosage dependency of the uptake and subcellular distribution of the metal in the olfactory epithelium and the brain. Toxicol Appl Pharmacol 1999;156:119–128.
17. Taylor AC, Weiss P. Demonstration of axonal flow by the movement of tritium-labeled protein in mature optic nerve fibers. Proc Natl Acad Sci USA 1965;54:1521–1527.
18. Goldstein LSB, Yang Z. Microtubule-based transport systems in neurons: the roles of kinesins and dyneins. Annu Rev Neurosci 2000; 23:39–71.
19. Drapeau P, Nachshen DA. Manganese fluxes and manganese-dependent neurotransmitter release in presynaptic nerve endings isolated from rat brain. J Physiol 1984;348:493–510.
20. Narita K, Kawasaki F, Kita H. Mn and Mg influxes through Ca channels of motor nerve terminals are prevented by verapamil in frogs. Brain Res 1990;510:289–295.
21. Taschenberger H, Jüttner R, Grantyn R. Ca^{2+}-permeable P2X receptor channels in cultured rat retinal ganglion cells. J Neurosci 1999;19: 3353–3366.
22. Tjälve H, Mejáre C, Borg-Neczak K. Uptake and transport of manganese in primary and secondary olfactory neurones in pike. Pharmacol Toxicol 1995;77:23–31.
23. Elluru RG, Bloom GS, Brady ST. Fast axonal transport of kinesin in the rat visual system: functionality of kinesin heavy chain isoforms. Mol Biol Cell 1995;6:21–40.